ARMA 17-644

# Phase-Field Modeling of Fracture in $CO_2$ Sequestration

Culp, D.
*University of Colorado, Boulder, Colorado, USA*
Tupek, M.R.
*Sandia National Laboratories, Albuquerque, New Mexico, USA*
Newell, P.
*University of Utah, Salt Lake City, Utah, USA*
Hubler, M.H.
*University of Colorado, Boulder, Colorado, USA*



**ABSTRACT:** This work studies fracture propagation in the encasements of wellbores, and how extreme pore pressures and pressure rates affect their damage states. The initiation and evolution of fractures in poroelastic media often gives rise to discontinuous fields within computational problems. Such models present computational challenges due to the complexity of sharp discontinuities that arise during the finite element solution and also lack the ability to model fracture initiation. These challenges may be alleviated by using a phase field formulation of fracture mechanics, which introduces a continuous, diffusive scalar damage field around crack surfaces. We make use of a direct computation of the crack's width, or joint opening, by using the gradient of the phase field in the damaged area. This is useful for determining the material's fluid-mechanical properties, such as the calculation of Poiseuille-type flow that occurs within a sufficiently damaged medium. Using this approach, it can be shown that the evolution of such fractures in a porous medium can contribute to the material's permeability, hence coupling fluid flow and damage within a material. Conversely, the movement of fluids through a damaged solid can influence the material's fracture distribution driven by pore pressures, meaning that there is a two-way coupling of damage and fluid flow. Using the Sierra Mechanics code suite at Sandia National Laboratories, a phase-field model of fracture is developed which will allow a loose, two-way coupling of these physics for future implementations. We find the model's ability to predict fractures initiated and propagated by increasing pore pressure to be consistent with fractures that occur from fluid injections. We also find that the joint openings calculated with this model will be helpful for implementing Poiseuille flow along fractures.

## 1. INTRODUCTION

### *1.1 Motivation*

The coupled physics of pressurized fluids in porous rock and fracture propagation is essential in subsurface rock mechanics. Applications in fields such as hydrology deal with the distributions of contaminants in groundwater, which are often dependent on fracture distributions in the earth's crust, and the phenomenon of fluid induced fault activation is of great interest in the field of geophysics. The concept of carbon sequestration is contingent upon pressurized fluids, and $CO_2$, being contained within poroelastic substrates of the subsurface. In **Martinez and Newell, 2015**, it is shown that under certain pressure conditions, $CO_2$ and brine will flow along existing joints and faults when an injection occurs at depth. This implies that the $CO_2$ intended to be sequestered may leak over time.

Because fracture is a failure mode that occurs on many scales, both temporally as well as spatially, the ability to enlist the help of parallel computation through finite elements simulations is important for predicting and modeling these scenarios. Quantifiable measures of failure, such as a material's damage, can be easily computed and tracked when running simulations. These

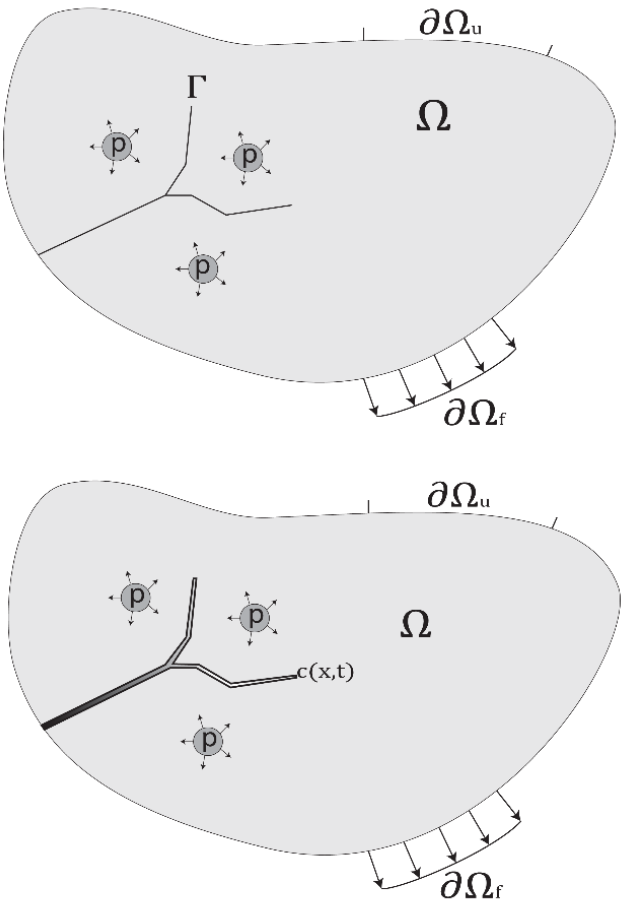


Fig. 1. A diagram representing a solid body Ω, under traction and displacement boundary conditions, $\partial\Omega_f$ and $\partial\Omega_u$ respectively, with crack surfaces represented as Γ, on the left while the phase-field approximation is represented as $c(x,t)$ on the right. Pore pressure, p, is included as a driving force.

quantities are not readily available when tests are conducted using physical experiments, nor are their time-scales reasonable for physical experiments, often spanning 10,000's of years.

Within this paper, a brief overview of the physical processes that are of interest are discussed, followed by a summary of a few methods that are often used to predict fracture. An in depth review of the phase-field method is discussed in chapter two to familiarize the audience with this model, while chapter three discusses the relationship between flow and fracture, and highlights the formulation of the joint opening vector. Chapter three describes the numerical tests that were run with the newly formed material model, with applications of injection of fluid into wellbores.

### *1.2. Deformation, Diffusion and Damage*

There are three important mechanical properties that are of interest in most subsurface rock mechanics problems: deformation, diffusion, and damage. In poroelastic media these properties are all connected by constitutive relations through the underlying physics. Figure 1 below depicts how these processes are related. Poroelasticity describes a porous material, with a solid matrix behaving elastically and interstitial fluids that behave viscously. The solid mechanics in such a medium are described using the constitutive laws of linear elasticity, and the fluid mechanics with Darcy's law of fluid transport.

The first pair of coupled properties that we will consider within a poroelastic solid is that of damage with deformation. When a solid is deformed, the effective stress within the solid is changed, so long as the surfaces are restrained to limit rigid body modes. When a portion of that solid has reached a critical threshold called the critical energy release rate, or $G_c$, a crack will propagate. Conversely when a fracture forms, the elastic strain energy is relaxed, which alters the displacement field of the solid. This coupled model of damage and deformation is formulated here in terms of a damage variable called phase-field.

Using Biot's linear theory of poroelasticity, the processes of fluid flow and fracture within a material can be coupled: the existence of cracks leads to fluid flowing along these joints known as Poiseuille flow, and conversely, an increase pore pressure, often due to fluid flow, may lead to initiation and/or further propagation of cracks, **Biot, 1972**.

It is also important to recognize the coupled mechanisms of fluid transport and displacement within a poroelastic medium, which has already been well established by Terzaghi and Biot in the 20th century, **Terzaghi, 1925**. An example of this is a porous, saturated rock that is not as easily compressed as one that is drained due to the presence of the additional pore pressures in the saturated rock. Biot's model of poroelasticty readily demonstrates the diffusion-and solid displacement.

### *1.3 Fracture within Solids*

The importance of understanding damage evolution has led to the development of numerous fracture models, many of which rely on Griffith's theory for brittle fracture, which relates a crack's nucleation and propagation to a critical energy release rate. Theoretical fracture models depend on a crack developing or propagating when this critical value is reached, leading to a process zone that transitions from completely undamaged to fully damaged at a single point **Borden et al., 2012** or over specified region **Camacho and Ortiz, 1996**.

There are various approaches to numerical modeling of fractures within solids. Of these approaches, several are robust in modelling different fracture scenarios, with reasonable computational expense. The extended finite element method (XFEM), enriches the finite element solution space with discontinuous fields associated with a crack independent of the mesh **Moes et al., 1999.** However, this approach does not specify the particular physics of fracture initiation and propagation, and

implementations in 3D are notoriously difficult due to the complexity of the required computational geometry.

Another approached based on the peridynamic theory assumes that particles within a body interact with each other in a nonlocal sense, within a finite neighborhood. In this model, fracture occurs as forces acting between material points are decayed to zero based on a predefined threshold, e.g., a critical stretch. The peridynamic equations of motion at a point involve an integral functional of the bond forces in a body. It is a continuum theory, which naturally discretizes as a mesh-free particle method **Silling and Askari, 2005**. In this aspect it is favorable over methods that treat cracks explicitly - because the equations of motion and the constitutive models naturally drive fracture initiation and propagation. The use of a pairwise force function is not the traditional method of representing constitutive relations, making the method inconvenient. It is also an oversimplification to assume that any two particles can be simply related with a single force potential **Foster and Silling, 2009.**

A Lagrangian finite element model for brittle materials based on cohesive zones was developed in the mid 1990's. This method is used to predict the propagation of discontinuities along the interface between elements based on a cohesive traction separation law. These models are a departure from brittle fracture, because cracks may develop from the gradual delamination of the crack surfaces. This process takes place in the cohesive zone, which represents an extended crack tip, and was originally formulated to avoid the crack tip stress singularity that is present in linear elastic fracture mechanics. A major advantage of the CZM over linear elastic fracture mechanics is the ability to predict behavior of initially undamaged material **Bažant and Li, 1995**. A disadvantage to such a method is the mesh-dependency of the fracture path **Camacho and Ortiz, 1996.**

### *1.4. Phase-field Modeling of Fracture*

In order to better deal with some of the aforementioned challenges, a phase-field model of fracture is implemented, whose basic motivation is to smooth out the crack surface discontinuity by using a diffusive scalar field, *c*. Figure 2 depicts how a variable, *c*, approximates a discontinuous function (the crack surface in this case). Since the crack is a natural outcome of the analysis it does not require an explicit geometric representation and tracking, which is an advantage over alternative techniques. This phase-field variable represents damage, and provides a diffuse transition between unbroken and broken material **Wheeler et al., 2013**. This damage variable is only defined in the set [0,1], and

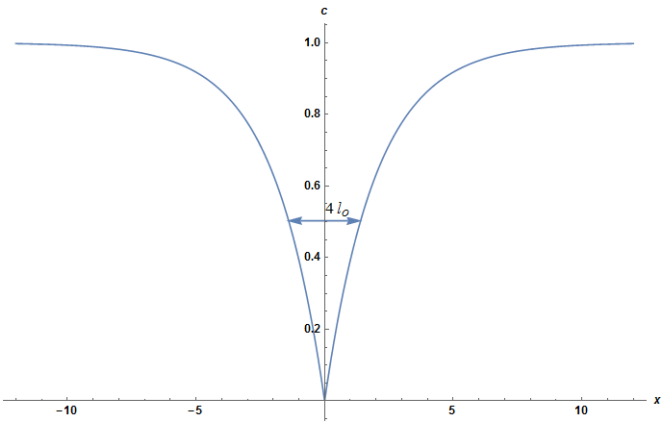


Figure 2: Phase-field approximation of a crack in 1-D. The damage parameter, c, portrays a fully damaged material at a value of zero, and is spatially smooth moving away from the crack. The length scale, $l_0$ , defines the width over which the crack is smoothed.

will take the value of 0 on the crack surface, while taking a value of 1 away from the crack.

For the implementation considered here, we use a fixed mesh to avoid the need for adaptive re-meshing. **Bourdin et al., 1999** show that the phase-field solution converges to linear elastic fracture mechanics as the length scale associated with the phase-field approaches zero.

## 2. PHASE-FIELD FORMULATION

### *2.1 Mathematical Formulation of Phase-Field Fracture Model*

We will consider the phase-field formulation which is based on a variational statement of brittle fracture. To do this, we first establish the potential energy of the system. For a linear-elastic, isotropic material, we consider the elastic strain energy density, $\psi_e(\boldsymbol{\epsilon})$, where $\boldsymbol{\epsilon}$ is the infinitesimal strain tensor, and both $\lambda$ and $\mu$ are the Lamé coefficients, as shown below in equation (2.1):

$$\psi_e(\boldsymbol{\epsilon}) = \frac{1}{2}\lambda\epsilon_{ii}\epsilon_{jj} + \mu\epsilon_{ij}\epsilon_{ij} \qquad (2.1)$$

In (2.2), the total potential energy, $\boldsymbol{\Psi}(\boldsymbol{\epsilon}, \boldsymbol{\Gamma})$, is considered, which is the sum of the elastic strain energy and fracture energy. Γ(t) represents a set of crack surfaces that exists within the body at some time t, while Ω is an arbitrary bounded domain. The fracture energy is calculated by multiplying the total crack surface area by $G_c$, the critical fracture energy **Lorentz et al, 2011**.

$$\boldsymbol{\Psi}(\boldsymbol{\epsilon}, \boldsymbol{\Gamma}) = \int_\Omega \psi_e(\boldsymbol{\epsilon}) d\Omega + \int_\Gamma G_c d\Gamma \qquad (2.2)$$

It is convenient to introduce a scalar variable, which we will call the phase-field variable *c*, in order to formulate a regularized formulation of the total potential energy above. We approximate the fracture energy as a volume

integral, rather than a surface integral, and can approximate our fracture energy with an integral of crack density function, $\gamma_l$, which is the integrand in (2.3) below **Miehe et al, 2010**.

$$\Gamma_{l_0}(c) = \int_\Omega \frac{1}{4l_0}[(c-1)^2 + 4l_0|\nabla c|^2]d\Omega \quad (2.3)$$

A user chosen length-scale variable, $l_0$, is introduced which specifies the width over which a fracture is smoothed from $c = 0$ to $c = 1$. **Borden et al, 2012** show that (2.3) is minimized, when the following Euler-Lagrange equation holds true:

$$c - 1 - 4{l_0}^2 \Delta c = 0. \quad (2.4)$$

In one dimension, the solution of differential equation (2.4) leads to:

$$c(x) = 1 - e^{-|x|/2l_0}, \quad (2.5)$$

which is depicted in Figure 2.

The approximation of (2.2) is finalized by considering the form of the elastic strain energy density function, $\tilde{\psi}(\epsilon, \Gamma)$. Following **Miehe et al. 2010**, we decompose $\psi_e$ into tensile and compressive energy contributions, shown as ${\psi_e}^+$, and ${\psi_e}^-$ respectively, and assume that the elastic strain becomes:

$$\tilde{\psi}(\boldsymbol{\epsilon}, \mathrm{c}) = c^2 {\psi_e}^+(\boldsymbol{\epsilon}) + {\psi_e}^-(\boldsymbol{\epsilon}). \quad (2.6)$$

This decomposition effectively removes any crack growth due to compressive stresses, which is a fair assumption for this application, leaving tension as the sole source of damage. The $c^2$ term is chosen as the damage coefficient, and is responsible for erosion of the elastic energy during tensile strains. Finally, we can consider the total potential energy approximation, $\widetilde{\Psi}$, inserting (2.3) and (2.6) into (2.2):

$$\widetilde{\boldsymbol{\Psi}}(\boldsymbol{\epsilon}, \mathrm{c}) = \int_\Omega \left[ \mathrm{c}^2 \psi_\mathrm{e}^+(\boldsymbol{\epsilon}) + \psi_\mathrm{e}^-(\boldsymbol{\epsilon}) + \frac{1}{4\mathrm{l}_0} \mathrm{G_c}[(1 - \mathrm{c})^2 + 4\mathrm{l}_0 |\boldsymbol{\nabla}_\mathrm{c}|^2] \right] \mathrm{d}\Omega \quad (2.7)$$

In order to impose the irreversible nature of crack growth into our model, a strain-history field, $\mathcal{H}$, is introduced which satisfies the Kuhn-Tucker conditions for loading and unloading and will replace the tensile contribution of strain energy when solving for the damage variable. This replacement addresses the idea that $c$ is a monotonically decreasing parameter, and a damaged material will not heal under compressive stresses. This can be expressed as in equation (2.8):

$$\frac{\partial c}{\partial t} \leq 0 \quad (2.8)$$

The corresponding kinetic energy of this arbitrary body is:

$$\Psi_{kin}(\dot{\boldsymbol{u}}) = \frac{1}{2}\int_\Omega \rho \dot{u}_i \dot{u}_i dx \quad (2.9)$$

The strong form of the problem at hand is outlined by **Borden et al, 2012,** where (2.10) and (2.11) describe the system of partial differential equations that are to be solved:

$$\left(\frac{4l_0 c\mathcal{H}}{G_c} + 1\right) c - 4{l_0}^2 \frac{\partial^2 c}{\partial x_i^2} = 1 \quad (2.10)$$

$$\frac{\partial \boldsymbol{\sigma_{ij}}}{\partial \boldsymbol{x_j}} = \rho \ddot{\boldsymbol{u}}_{\boldsymbol{i}}, \quad (2.11)$$

where $\ddot{u}$ represents the second derivative of position with respect to time, or acceleration. As a broad review of the derivation, (2.10) and (2.11) fall out of the Lagrangian energy functional, after setting variations with respect to both the displacement and phase field equal to zero. Note that (2.11) is simply a statement of the conservation of momentum from the classical continuum theory. These equations are solved using a staggered solution procedure in order to find the displacement field and phase-field given the following boundary and initial conditions:

$$(BC) \begin{cases} u_i = g_i \\ \sigma_{ij} n_j = t_i \\ \frac{\partial c}{\partial x_i} n_i = 0 \end{cases} \quad (2.12)$$

$$(IC) \begin{cases} \boldsymbol{u}(\boldsymbol{x}, 0) = \boldsymbol{u}_0(\boldsymbol{x}) \\ \dot{\boldsymbol{u}}(\boldsymbol{x}, 0) = \boldsymbol{v}_0(\boldsymbol{x}) \\ c(\boldsymbol{x}, 0) = c_0(\boldsymbol{x}), \end{cases} \quad (2.13)$$

where $g_i$ and $t_i$ are prescribed on $\partial\Omega_u$ and $\partial\Omega_f$, while $\boldsymbol{u}_0$, $\boldsymbol{v}_0$ and $c_0$ prescribed in $\Omega$.

### *2.2. Energy Release Rate*

According to Griffith's model of fracture mechanics, a crack will propagate if the rate of elastic strain energy decreases at a rate that is equal to the critical energy release rate, **Griffith, 1921**. Within the phase field model, this value, $G_c$, can be used to determine certain properties of interest including the maximum stress, $\sigma_c$, which can be achieved in the material.

$$\sigma_c = \frac{9}{16}\sqrt{\frac{EG_c}{6l_0}} \quad (2.14)$$

## 3. POROUS FLOW

### *3.1. Overview of numerical methods*

The numerical models in these studies make use of Sierra Mechanics, **Shaw et al., 2015,** developed at Sandia National Laboratories, which is an engineering mechanics simulation framework that has been developed to study computational mechanics using MPI parallel finite element discretization. A variety of rock mechanics problems can be addressed with this suite of codes, and of particular interest to this work is the solid mechanics module called Adagio, and the fluid mechanics module called Aria. These two modules are coupled via data transfers within each time step. In this case, the variables which are passed between the codes are pore pressure and effective stress. This loose, two-way coupling will be achieved through Arpeggio, which acts as a courier between the two modules within Sierra.

Within Sierra's material library, LAME, a C++ material class called "Phase-field Porous Flow" was created in order to run simulations for fracture and flow problems, based on a phase field approach to handle the crack propagation as described above. This material model modifies the standard phase field model in two critical ways: 1) the total stress is augmented by the hydrostatic term, as seen in (3.1), and 2) the joint opening vector is computed from the phase and which will be used to update a material's permeability. The following sub-sections detail these processes.

### *3.2. Two-way coupling of flow and fracture*

Rather than considering a bulk approach to the coupling of fluids and solids in poroelastic media, we will consider the two phases separately during each time-step and update these properties with a loose coupling. By implementing the constitutive relations independently of one another, we are able to model the effective stress, and stress contribution of the fluid pressure. We do this to take the individual contributions of its solid and fluid constituents into account, preventing the need to lump the states' parameters into one model and lose sensitivity to a change in a material's porosity or fluid content. Because we are considering a two-way coupling between fluid flow and damage, a formulation of how each field is updated is required. Let us first consider how the phase-field variable is modified by the onset of fluid flow with a medium. By solving (2.10) and (2.11), we are able to compute the damage field within the medium, given a particular state of stress. When considering a porous, fluid saturated material, equation (3.1), is needed to incorporate the hydrostatic pressure of the fluid filling the pore-spaces.

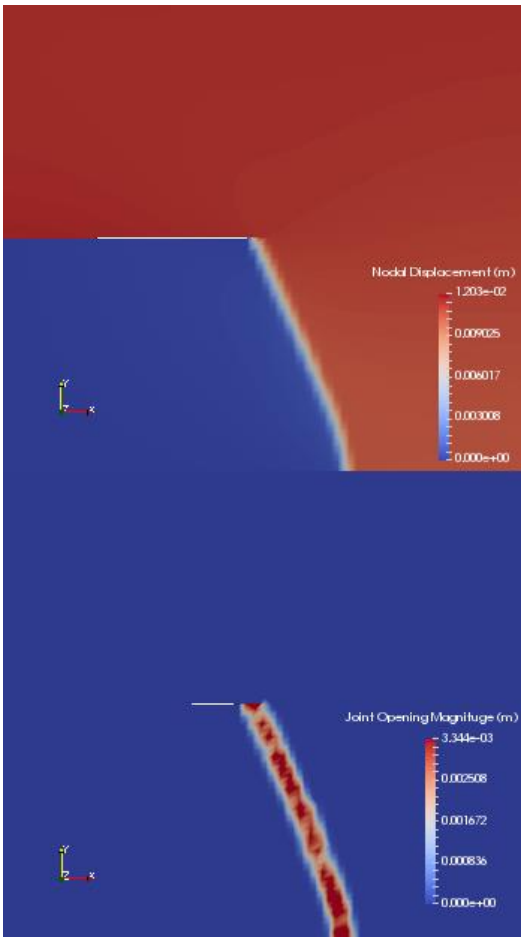


Fig. 3. Computational results showing displacements, top, and the magnitude of the joint opening vector, bottom, when a solid is subjected to a Mode-II failure. Notice the correlation of these magnitude in the neighborhood of the fracture

where $\boldsymbol{\sigma}$ is the total stress, $\tilde{\boldsymbol{\sigma}}_{\boldsymbol{eff}}$ is the effective stress in the solid skeleton, b is the Biot's coefficient and p is the

$$\boldsymbol{\sigma} = c^2\tilde{\boldsymbol{\sigma}}_{\boldsymbol{eff}} - bp\mathbf{1}, \tag{3.1}$$

fluid pressure or pore pressure. Including the hydrostatic pressure in (3.1) performs the task of one half of the two-way coupling of damage and flow, by modifying the damage as a function of pore pressure. The second half of the coupling will occur when the permeability is updated as a function of aperture of fractures.

Within LAME, a joint opening vector is computed as a field variable over the elements in the model using the spatial gradient of the phase field variable. This state variable will allow the computation of Poiseuille-type flow through cracks and couple the flow to the solid mechanics portion of the simulation. The joint opening state variables can be summarized by the equations below, in which $\boldsymbol{\lambda}_{\perp}$ represents the stretch perpendicular

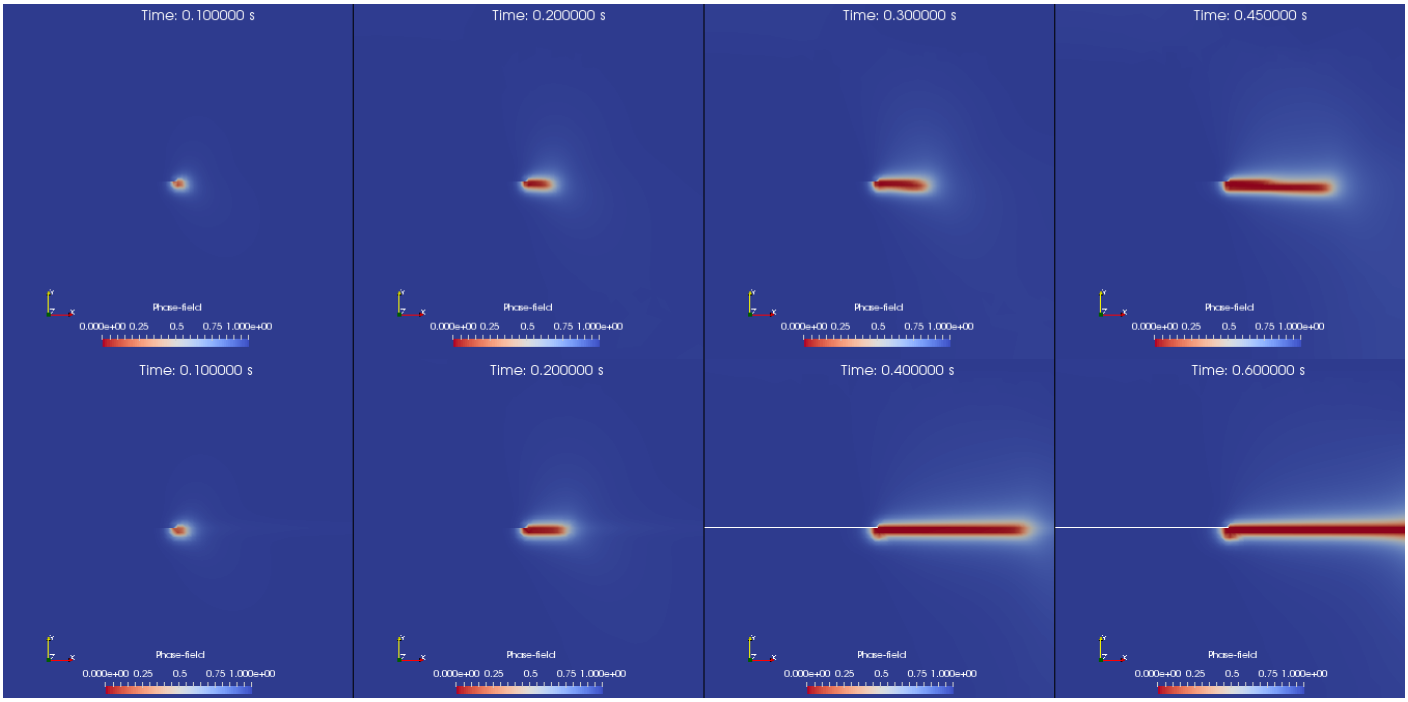


Fig. 4. The top shows computational results tracking phase-field, *c*, under a Mode-I failure scenario over time. The bottom depicts the same sample with the additional loading due to pore pressures which are ramped up in the expected area of failure

to a crack, while $\nabla \mathbf{c}$ represents the gradient of damage, and $\boldsymbol{C^{-1}}$ is the inverse of the Right-Cauchy Green tensor in (3.5). The crack opening width represented by $\omega$, is formed from a product of the element length in the neighborhood of the crack, $L_{\perp}$, and an adjusted stretch vector. As (3.6) indicates, this value is zero unless the phase-field is less than some user-chosen threshold value, $c_0$. Ultimately, the joint opening vector $\vec{\boldsymbol{\delta}}_{\boldsymbol{n}}$ , the state variable of interest, is formed by scaling the unit vector normal on the deformed crack surface , $\hat{\mathbf{n}}$, by the crack opening as shown in 3.7). These equations have been modified from **Miehe et al.'s 2015** work.

$$\boldsymbol{\lambda}_{\perp}^{2} = \frac{\nabla \mathbf{c} \cdot \nabla \mathbf{c}}{\nabla \mathbf{c} \cdot \mathbf{C}^{-1} \cdot \nabla \mathbf{c}} \tag{3.5}$$

$$\omega^{2} = \begin{cases} (\lambda_{\perp}\text{-}1)^{2}\, L_{\perp}^{2} \\ 0 \end{cases} \quad \text{for } c < c_0, \tag{3.6}$$

$$\vec{\boldsymbol{\delta}}_{\mathbf{n}} = \omega \hat{\mathbf{n}} \tag{3.7}$$

In order to assess the accuracy of this field variable, the nodal displacements in a Mode-II failure scenario is simulated where the nodal displacements in the neighborhood of a fracture are compared to the magnitudes of the joint opening vectors on each element. Figure 3 shows that these values are within 10% of one another, confirming that the crack's aperture is relatively close to the material displacements near the crack.

## 4. NUMERICAL INVESTIGATIONS

### *4.1 Description of Finite Elements*

The purpose of these investigations was to explore the effects of increasing pore pressure on a material's fracture distribution, as well as demonstrating the computed joint opening field associated with the solid's phase-field estimation of fracture. In the following examples, 8-node hexahedron elements were used in order to spatially discretize the domain.

The phase-field formulation described earlier, along with the displacement field, are solved using an explicit time-staggered integration, utilizing an implicit solver for the parameter *c*, **Shaw et al., 2015**. Similar solution methods are detailed in **Borden et al., 2012**. It is worth noting that the following investigations are similar to those of **Miehe et al., 2015** and **Mikelic et al., 2015**, however, there they use 2-D quadrilateral elements. A length scale, $l_0 \approx 2h$ suggested **in Miehe et al., 2010** has provided the best spatial resolution when computing fractures using mesh size $h$. The time step is chosen to be $\tau = 0.01\ s$ unless otherwise noted. Upon determination of the fracture prone regions, these areas were refined and biased in order to provide improved spatial resolution of the joint opening and phase-field variables. Table 1 lists several of the defining parameters, which have been chosen to represent typical subsurface properties found in many rock types, for the following numerical problems.

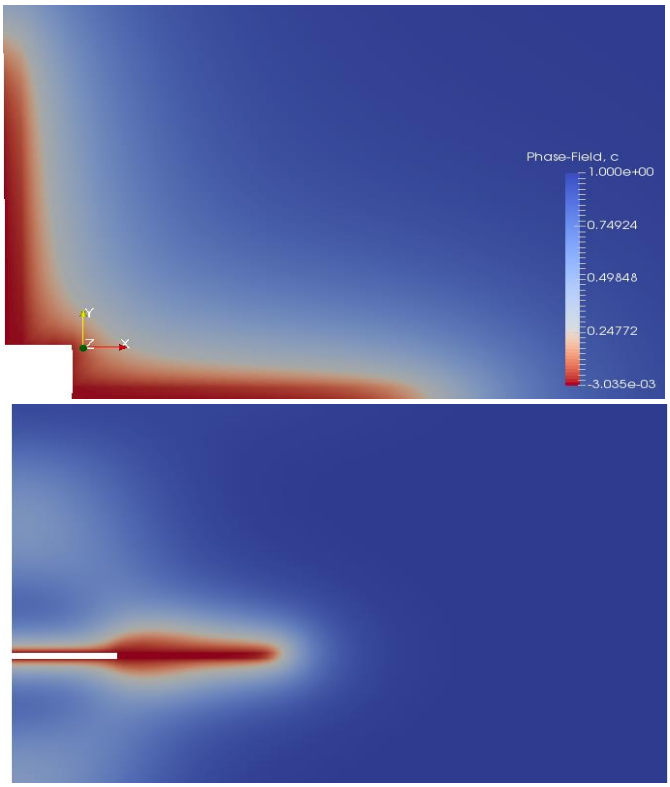


Fig. 5 The evolution of a phase-field prediction of fracture induced by two well-bore scenarios. The vertical orientation is shown on top, and the horizontal on the bottom.

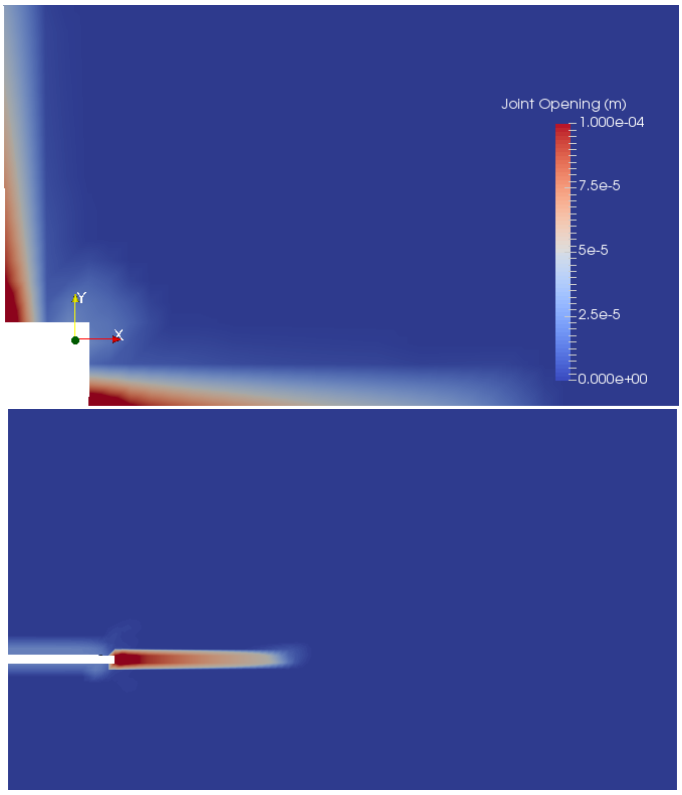


Fig. 6 The evolution of the joint-opening along the crack in a vertical well-bore scenario (top) and a horizontal well-bore (bottom). In both scenarios, fracture is initiated by the stress created from pore pressure injections of the same magnitude. The injection areas are shown in white.

### *4.2 Mode-I fracture*

This boundary value problem explores the phase-field solution to a Mode-I failure due to prescribed linear displacements on the boundary of our domain. In this example, there is an initial separation between the top and bottom halves of the domain imposed from the left surface to the center of the mesh. Displacements in Z are restrained, while the top and bottom (in terms of Y) are restrained in both X and Y displacements. A displacement in Y is applied to the top half of the mesh, which causes the mesh to open and a crack to propagate.

Figure 4 demonstrates the results of monitoring the phase-field variable of a material subjected this Mode-I fracture, during which a joint forms perpendicular to the direction of spreading. The bottom of this figure shows the effect of increasing pore pressure over time in the portion of the domain where a fracture forms. Due to the higher total stress in this area under pore pressures, the phase-field approximation of fracture increases at a much faster rate in the scenario with pore pressure injection.

### *4.3 Fracture due to well-bore orientation*

In these tests, we want to model a vertical well-bore with an injection zone that is symmetric in plan-view. The domain is set up as a mesh of 100 x 100 x 1 eight-node hexahedral elements. This mesh appears to be sufficiently large to avoid boundary effects arising from the far-field boundary conditions. In this scenario we assume quarter symmetry about the X and Y axes, and model our injection zone as a square block of sixteen hexahedral elements at the origin. By using quarter symmetry on the mesh, we are able to decrease the computational cost. The size of the domain has been set up to be 0.5 m. x 0.5 m. x 0.005 m. and all surfaces are restrained from vertical displacement (Z-direction), while the surfaces normal to X and Y are restrained in the X and Y directions.

Material values were chosen to represent limestone, with a density of 2250 Kg/m$^3$, a Young's modulus of 7 x10$^9$ Pa and a Poisson's ratio of 0.155. The fracture energy release rate parameter was chosen to be $G_c = 98\ \frac{J}{m^2}$.

A simulation time of 1 s was chosen, and discretized into 50 time steps with $\tau = 0.02$ s over which the pore-pressure is ramped linearly. In these studies, the slope of this pore pressure ramp-up is varied, while the times until fracture initiation, maximum and average joint opening magnitudes, and fracture lengths are recorded. We define fracture initiation when the phase-field parameter, $c$, is less than 0.1 at some node on the mesh. In addition to linearly increasing the pore-pressure over time, introducing a constant pore pressure at $t$=0, equal to the final values in the linear tests, was also performed. It was

concluded that the true driving factor of the joint opening magnitude in these scenarios is the final pore pressure, and not the rate at which it is introduced.

Another possible fluid-injection orientation, is that of a horizontal well-bore, in which the injection zone has a higher aspect ratio than that of the vertical well-bore scenario. To capture this, the injection zone was modeled

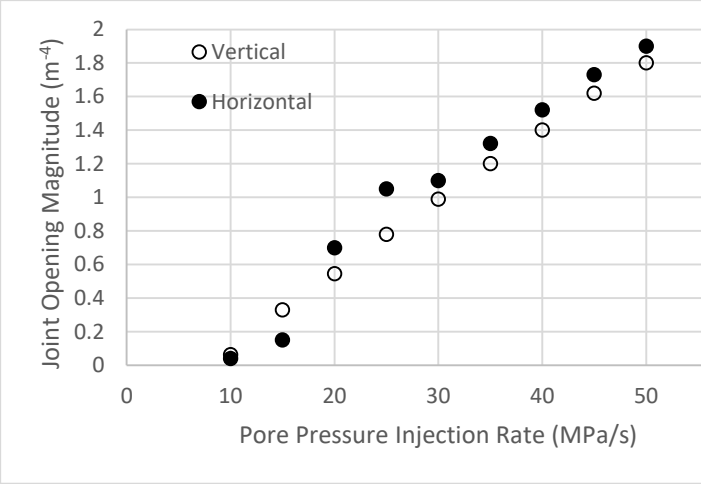


Fig. 7 Joint opening magnitude is shown for the two different well-bore scenarios, over increasing pore-pressure injection rates.

with a block of elements arranged in a line, and centered on the left (X) side of domain. Half-symmetry is satisfied using this arrangement, and we also preserve the same volume for the injection well, 0.02 $m^3$. Figure 5 shows the phase-field solution of two well orientations with a pore pressure injection rate of 30 MPa/s, while figure 6 shows their joint opening magnitudes at the end of the tests.

Figure 7 shows the results of this analysis. It should be noted that both sets of data initially behave linearly with increasing pore pressure before the meshes experience a critical amount of damage, at which point the joint openings plateau. The magnitudes in both scenarios are very close to one another and follow the same linear trend. Because the same volume is considered within each injection zone scenario, we would expect to see similar results from the two well-bore orientations. Additional simulations were run involving final pore pressures below 10 MPa, however, these pore pressures did not create enough damage to initiate fractures. On the other hand, scenarios with final pore pressures greater than 50 MPa created boundary effects, which made the results inconclusive.

## 5. CONCLUSION

By using the phase-field approximation of fracture, insight can be gathered about the characteristics of poro-elastic materials under different types of stress. Using this model, it has been shown that the vertical and horizontal injection scenarios produce similar joint opening magnitudes, and both show similar linear patterns of increased magnitude with increased pore pressures. Fracture initiation can be observed across many length-scales which is important when considering fracture and fluid flow within geo-materials. In the future, this work will lend useful in a loose two-way coupling of porous flow and the phase-field model for fracture. In particular, the joint opening vector described in this paper will be used to model the Poiseuille flow that occurs when such materials are fractured. Future efforts will be made to implement such a model coupled with geo-material models to study the long term effects of pressurized fractures within the earth, with further applications to be considered in the realm of carbon sequestration.

Table 1 showing values used in numerical investigations

| **Parameter** | **Symbol** | **Value** |
|---|---|---|
| Young's Modulus | E | 10 GPa |
| Density | $\rho$ | 2560 $\frac{kg}{m^3}$ |
| Critical Fracture Energy | $G_c$ | 100 $\frac{J}{m^3}$ |
| Fracture Length Scale | $l_0$ | 0.02 m. |
| Poisson Ratio | $\nu$ | 0.155 |
| Biot's Coefficient | $b$ | 1 |
| Edge Length of Hex Element | $h$ | 0.01 m. |

## REFERENCES


1. Borden, M.J., C.V. Verhoosel, M.A. Scott, T.J.R. Hughes, C.M. Landis, A phase-field description of dynamic brittle fracture, *Comput. Methods Appl. Mech. Eng.* 217–220 (2012) 77–95.
2. Miehe C., S. Mauthe, Phase field modeling of fracture in multi-physics problems. Part III. Crack driving forces in hydro-poro-elasticity and hydraulic fracturing of fluid-saturated porous media, *Comput. Methods Appl. Mech. Engrg*. 304 (2016) 619–655
3. Martinez, M., P. Newell, Coupled multiphase flow and geomechanics model for analysis of joint reactivation during CO2 sequestration operations, *International Journal of Greenhouse Gas Control* 17 (2013) 148–160
4. Bourdin, B., G. A Francfort, and J.-J. Marigo. The variational approach to fracture. *Journal of elasticity*, 91(1-3):5–148, 2008.
5. Moës, N., J. Dolbow, T. Belytschko, A finite element method for crack growth without remeshing, *Int. J. Numer. Methods Engrg.* 46 (1) (1999) 131–150.
6. Mikelic, Andro, Mary F. Wheeler, and Thomas Wick. A phase-field method for propagating fluid-filled fractures coupled to a surrounding porous medium. *Multiscale Modeling & Simulation*, 13(1):367–398, 2015.
7 Francfort, G.A. and J.-J. Marigo. Revisiting brittle fracture as an energy minimization problem. *Journal of the Mechanics and Physics of Solids*, 46(8):1319 – 1342, 1998.
8. Bažant ZP, Li Y. Stability of Cohesive Crack Model: Part I—Energy Principles. ASME. J. Appl. Mech. 1995;62(4):959-964. doi:10.1115/1.2896029.
9. Griffith, The phenomena of rupture and flow in solids., *Philos. Trans. R. Soc. Lond*. 221 (1921) 163-198.
10. Wheeler, Mary, Thomas Wick, Winnifried Wollner, An Augmented-Lagrangian Method for the Phase-Field Approach for Pressurized Fractures, ICES REPORT 13-25, The Institute for Computational Engineering and Sciences, The University of Texas at Austin, August 2013.
11. Camacho, G.T. and M. Ortiz. Computational modelling of impact damage in brittle materials. *International Journal of Solids and Structures*, 33(2022):2899 – 2938, 1996. ISSN 0020-7683. doi: http://dx.doi.org/10.1016/0020-7683(95)00255-3.
12. Borden, M. J., T. J.R. Hughes, C. M. Landis, and C. V. Verhoosel. A higher-order phase-field model for brittle fracture: Formulation and analysis within the isogeometric analysis framework. *Computer Methods in Applied Mechanics and Engineering*, 273:100
13. Miehe, C., M. Hofacker, F. Welschinger, A phase field model for rate-independent crack propagation: robust algorithmic implementation based on operator splits, *Comput. Methods Appl. Mech. Eng.* 199 (45–48) (2010) 2765–2778.
14. Lorentz, Eric, S. Cuvilliez, and K. Kazymyrenko. Convergence of a gradient damage model toward a cohesive zone model. *Comptes Rendus M´ecanique*, 339(1):20–26, 2011.
15 Silling, S.A., E. Askari, A meshfree method based on the peridynamic model of solid mechanics, *Computers & Structures*, Volume 83, Issues 17–18, June 2005, Pages 1526-1535, ISSN 0045-7949
16. Foster, J., S. A. Silling and W. W. Chen, State based peridynamic modeling of dynamic fracture 2 (2009) 1529-1535
17. Terzaghi, K., Erdbaumechanik auf bodenphysikalischer Grundlage, F. Deuticke, 1925.
18. Biot, M. Theory of finite deformations of pourous solids, Indiana Univ. Math. J. 21 (1972) 597–620.
19. Shaw, Ryan, Anthony M. Agelastos, Joel D. Miller, Guide to Using Sierra, SANDIA report SAND2015-1642, March 9, 2015

ACKNOWLEDGEMENTS

This material is based upon work supported by the U.S. Department of Energy, National Energy Technology Laboratory under Award Number DE-FE0026514.

Sandia National Laboratories is a multi-program laboratory managed and operated by Sandia Corporation, a wholly owned subsidiary of Lockheed Martin Corporation, for the U.S. Department of Energy's National Nuclear Security Administration under contract DE-AC04- 94AL85000.